ORIGINAL PAPER

Activated Carbon From Palm Fibres Used as an Adsorbent for Methylene Blue Removal

Lana S. Maia[1] · Andressa I. C. da Silva[1] · Emanuel S. Carneiro[1] · Francisco Maciel Monticelli[2] · Fernanda R. Pinhati[1] · Daniella R. Mulinari[3]

Abstract

In this paper, activated carbon was synthesized by chemical activation using sodium hydroxide as an activating agent from residues of the stem and sheath palm fibres, and their efficacies in the removal of methylene blue were evaluated. The materials were characterized by techniques like thermogravimetric analysis (TGA), Fourier transform infrared spectroscopy (FTIR), X-ray diffraction (XRD), scanning electron microscopy (SEM), and surface area (BET). The influence of two experimental factors, such as contact time (10 to 70 min) and initial dye concentration (25, 50, 100, 250, and 500 mg.L^{-1}) was investigated. The adsorption process was followed by the Langmuir isotherm model with a maximum adsorption capacity of 110.79 and 162.54 mg.g^{-1}for stem and sheath palm. Results demonstrated that activated carbon from palm fibres have characteristics necessary for the removal of methylene blue. The equilibrium data were well adjusted in the Langmuir isotherm model, which confirms that the adsorption was heterogeneous and occurred through physicochemical interactions.

Graphic Abstract
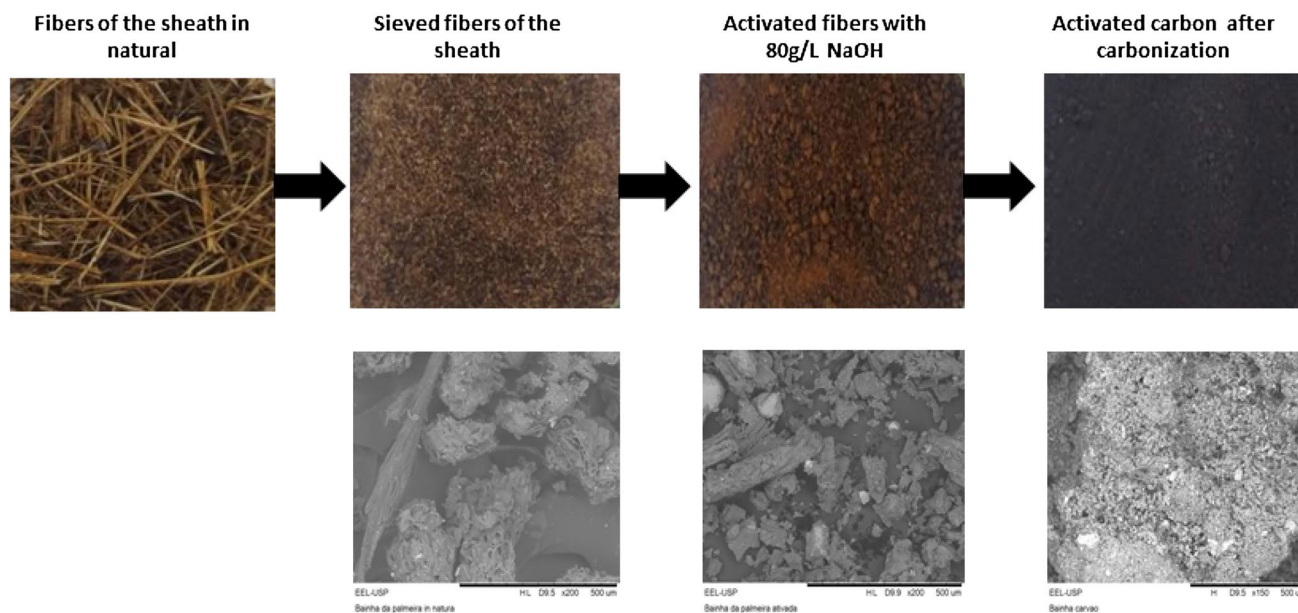
✉ Daniella R. Mulinari
dmulinari@hotmail.com; daniella.mulinari@fat.uerj.br

Extended author information available on the last page of the article

Introduction

The concern with wastewater generated by industries has stimulated the development of new technologies [1]. In this context, attention has been given to industrial effluents containing organic dyes, heavy metals, and contaminants, affecting water quality [2].

In Brazil, the National Environment Council (CONAMA) of the Environment Ministry establishes the disposal of liquid effluents. The CONAMA Resolution 430 regulates the conditions, parameters, standards, and directives to manage effluent releases into receptor water bodies, partially changing and complementing Resolution 357 [3, 4]. Effluents from any polluting source may be directly released into receptor bodies after their duly treatment and demands established in this Resolution and by other applicable standards.

One of the industrial pollutants of wastewater is the dye, extensively used in multiple industries such as textile, printing, cosmetics, ink, and plastics.

Among the various dyes, methylene blue (MB) is a cationic dye in the phenothiazine class and has various applications in chemistry, biology, and medicine [5, 6]. Exposure to MB can cause harmful health effects, such as high blood pressure, gastrointestinal pain, and nausea. Several methods are used to eliminate pollutants from aquatic environments, including coagulation-flocculation, precipitation, and oxidation [7, 8]. However, these methods are expensive and produce dangerous by-products [9].

Thus, adsorption has been the most used treatment process. Several studies focused on the adsorption of MB using activated carbon from vegetable fibres [6, 8, 10–12].

Activated carbon is the most widely used adsorbent due to its excellent color removal efficiency. However, the coal has an electrically positive surface, making the adsorption of cationic dyes difficult [12]. The use of agro-industrial waste is an alternative to developing low-cost adsorbents, contributing to reducing waste disposal costs. Among the various materials used to develop carbon, natural fibres originating from agro-industrial wastes are highlighted because they are renewable sources available at a low cost [13]. Consequently, activated carbon prepared from a large number of agro-industrial wastes such as coffee [14], pineapple plant leaves [15], pine cone [16], date palm leaflets [17] rice husk [18], apple peels [19], among others [20–24]. These wastes are found to be the most appropriate precursors due to their higher percentage of carbon and a lower amount of ash content [21].

Among the various natural fibres, palm fiber is a very abundant agro-industrial residue in Brazil and may have many more applications [25–27]. The heart of palm, also known as palmetto, can be extracted from various species of palms. *Archontophoenix alexandrae* produces the heart of palm of the noble type, with higher quality and superior flavor than other species of palm. For each palm, approximately 400 g of commercial palm heart is harvested. The residue constitutes 80 to 90% of the total palm weight, with some variation depending on the species [26]. According to the Brazilian Institute of Geography and Statistics (IBGE), the production of palm in Brazil was approximately 107.9 thousand tons, representing about 86.3 thousand tons of waste generated in 2018 [28].

The residues from king palm are mainly the leaves and leaf sheaths. Some quantity of this highly cellulosic material is currently used as boiler fuel to prepare fertilizers or as mulching material, but the majority is left on the mill premises [27]. However, the accumulation of this waste can generate environmental problems. Several studies seek to add value to this raw material produced from the extraction of palm heart by using it in other ways [26].

In this work, activated carbons prepared by chemical activation with NaOH from residues of the stem and sheath palm fibres for methylene blue removal. The materials were characterized by techniques like thermogravimetric analysis (TGA), Fourier transform infrared spectroscopy (FTIR), X-ray diffraction (XRD), scanning electron microscopy (SEM), and surface area (BET). The two experimental factors were investigated, such as contact time (10 to 70 min) and initial dye concentration (25, 50, 100, 250, and 500 mg.L-1).

Materials and Methods

Materials

Palm fibres (stem and sheath) were kindly provided by Biosolvit S/A, Rio de Janeiro/ Brazil. Royal palm, also known as *Archontophoenix alexandrae*, is a species originated from Australia, Oceania. In Brazil, its production stands out in the South and Southeast regions. Firstly, fibres were dried at 80 °C for 24 h for moisture removal. The fibres were ground in a mill and sieved to obtain samples that passed through 35 mesh screens.

Preparation of Activated Carbon

In this work, a method for the development of activated carbon from palm fibres using physical-chemical activation was performed, with chemical treatment and pyrolysis. Firstly, the fibres were dried in an oven at 80 °C for 24 h. Then, the palm fibres were impregnated with NaOH (80 g.L^{-1}) as an active agent (weight ratio 1/1) and dried at 100 °C for 24 h. Subsequently, the material was pyrolyzed in a muffle furnace under the inert atmosphere, flowing with 100 mL.

min^{-1} of argon, where the material was exposed to 400 °C for 3 h. After activation, the activated carbon was washed with distilled water, neutral pH, to remove the active agent and clear the formed pores (Fig. 1). Alkaline activation was used due to the synergistic effects between chemical activation and pyrolysis to fully expose the active adsorption sites and increase functional groups through the reaction between the carbon-oxygen and alkaline bond, increasing the adsorption capacity of the product [29–31]. In activated carbon preparation, the yield was defined as the final weight of activated carbon produced after activation, washing, and drying, divided by the initial weight of raw palm fibres.

Characterization of Activated Carbon

The proximate analysis of the raw palm fibres (stem and sheath) was carried out to determine the mass of moisture and ash of the *in natura* palm fibres (stem and sheath). The ultimate analysis to determine the mass of carbon, hydrogen, nitrogen, sulfur, and oxygen (C, H, N, S, and O) of the raw palm fibres (stem and sheath) and activated carbon was performed using the CHNS-O analyzer Flash 2000.

The morphology of the raw palm fibres (stem and sheath) and activated carbon were analyzed by Scanning electron microscopy (SEM), using a microscope HITACHI with tungsten filament operating at 5 kV, employing a low-vacuum technique and a secondary electron detector. Samples were dispersed on brass support and fixed with a double face 3M tape.

Diameter size distribution and surface area were determined using mercury porosimetry equipment from Quantachrome Instruments®. Hg porosimetry was used with were 241 kPa of pressure, 20 s of dwell time, and a vacuum of 25 kPa. Parameters were used to ensure no compressibility in the material during analysis.

The chemical structures of the raw palm fibres (stem and sheath) and activated carbon were analyzed by attenuated total reflectance Fourier transform infrared (ATR-FTIR) spectroscopy. The analysis was performed in a transmittance mode, in a range of $4500 − 400$ cm^{-1}, at the resolution of 4 cm^{-1}.

The physical structures of the raw palm fibres (stem and sheath) and activated carbon were evaluated by X-ray diffraction using a Shimadzu diffractometer, model XDR-6100. The measuring conditions were: CuKa radiation with graphite monochromator, 30 kV voltage, and 40 mA electric current. The patterns were obtained in 10–50° angular intervals with 0.05 steps and 1 s of counting time.

The fibres' thermal behavior and activated carbon were examined by performing the thermogravimetric analysis (TGA). This test method computes the weight loss incurred in the materials with temperature in a controlled atmosphere. Measurements were made by subjecting the material to a temperature range of 25–600 °C. TGA was conducted using SII Nanotechnology INC, model Exstar 6000 at a heating rate of 10 °C/min in a nitrogen atmosphere, and specimen weight of 10 mg.
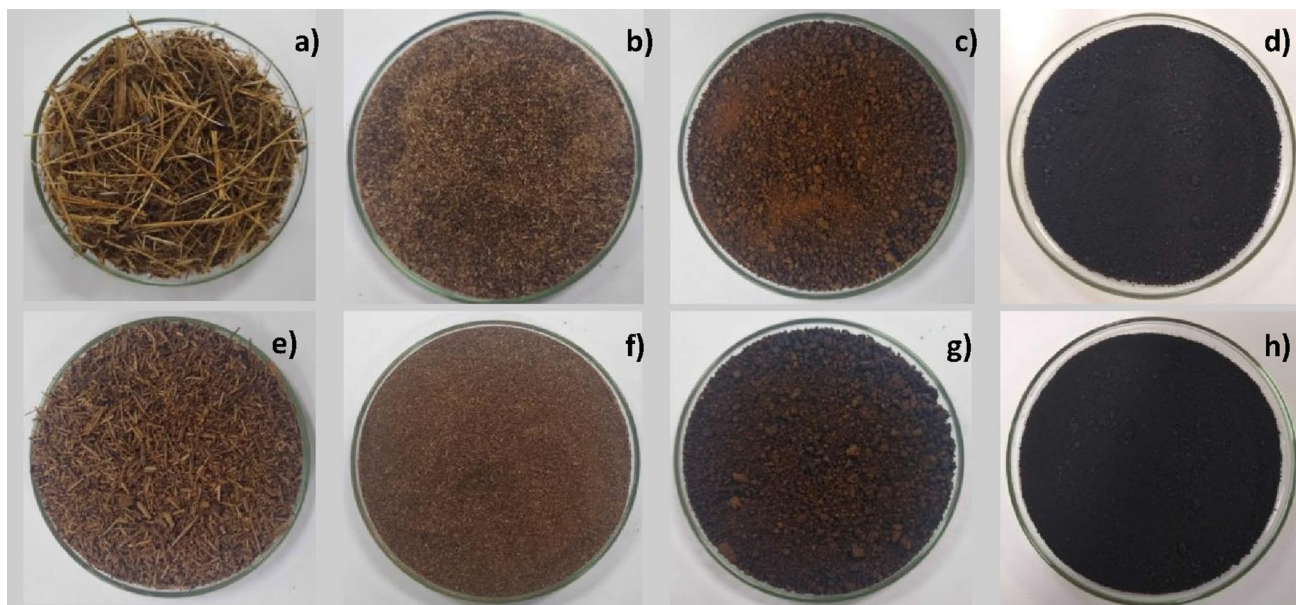

Fig. 1 Specimens from fibres stem and sheath from palm: **a** Fibres of the sheath *in natura*; **b** Sieved fibres of the sheath; **c** Activated fibres of the sheath; **d** Activated carbon of the sheath; **e** Fibres of the stem *in natura*; **e** Sieved fibres of the stem; **f** Activated fibres of the stem; **g** Activated carbon of the stem

Removal Methylene Blue

The method used for the measurement of methylene blue (MB) sorption capacity of the sorbent was based on the research developed by Pathania et al. [12]. The methylene blue sorption capacity from activated carbon was studied under a dynamic system. The sorbent (30 mg) was immersed in 100 mL of the aqueous methylene blue solution in the concentration range of 25, 50, 100, 250, and 500 mg.L^{-1}. The adsorption process was followed for 1 h under mechanical agitation in a shaker (40 rpm). To determine the pH value at the point of zero charge (pH$_{zpc}$), 0.1 g of activated carbon was added into 50 mL of 0.1 mol.L^{-1} NaCl solution. The pH was then adjusted to 2.0–10.0 by 0.1 mol.L^{-1} HCl or NaOH solution. After 24 h, the final pH values of the solution were measured. The pH$_{zpc}$ was the point at which pH$_{initial}$ equaled pH$_{final}$. The dye concentration in the solution was observed using a UV–visible spectrophotometer referring to the standard curve of methylene blue at the maximum wavelength of 665 nm. The quantity of dye adsorbed onto adsorbent (q$_e$,mg.g^{-1}) and removal (%) of MB were calculated using Eqs. (1) and (2), respectively:

$$q_e = (C_0 - C_e)\frac{V}{M} \tag{1}$$

$$\%Removal = \frac{C_i - C_e}{C_i}.100 \tag{2}$$

where: q$_e$ quantity of dye in mg per gram of adsorbent; C$_i$ and C$_e$ are respectively initial concentration and equilibrium time of MB (mg.L^{-1}); V volume of the solution; M mass of adsorbent.

Also, the effect of contact time in the removal efficiency of methylene blue sorbent was evaluated. The sorbent (30 mg) was immersed in 100 mL of the aqueous solution of methylene blue in the concentration 50 mg.L^{-1} under mechanical agitation in a shaker (40 rpm) in different times (10, 20, 30, 40, 50, 60 and 70 min).

Adsorption Isotherm

Adsorption isotherms can demonstrate the interaction between adsorbates and adsorbents, where the equilibrium distribution of adsorbate molecules occurs between the liquid and solid phases at a typical temperature [32]. The adsorption data were fitted to Langmuir isotherm model. Langmuir sorption isotherm is employed for equilibrium sorption, assigning monolayer sorption on a surface with a finite number of identical sites [12]. Experimental data were treated using a Wolfram Mathematica version 11.0, a software with extensive internal functionality for graphics,

linear algebra, and direct implementation. Besides, this software offers an intuitive environment and visualization functions. Therefore, it is an ideal package for educational or research purposes [33, 34]. The Langmuir equation can be written by Eq. 3:

$$\frac{1}{q_e} = \frac{1}{q_m} + \frac{1}{K_l q_m C_e} \tag{3}$$

Thus, the shape of this isotherm can also be expressed in terms of separation factor (RL), which can be given by Eq. 4:

$$RL = \frac{1}{1 + K_L C_e} \tag{4}$$

where: K$_L$ is Langmuir constant (L.mg^{-1}) related to the affinity of binding sites and the free energy of sorption; q$_e$ is dye concentration at equilibrium onto biosorbent (mg.g^{-1}); C$_e$ is dye concentration at equilibrium in solution (mg.L^{-1}); q$_m$ is dye concentration when monolayer forms on biosorbent (mg.g^{-1}); RL is a separation factor.

In several adsorption situations, adsorbate (favors) solid to liquid phase and adsorption is said to be favorable, 0 < RL < 1. When RL > 1, there is an indication that the solute (favors) liquid to the solid phase. RL = 1 corresponds to a linear isotherm [35].

Results

Characterization of Activated Carbon

The chemical compositions of the *in natura* palm fibres (stem and sheath) used in activated carbons preparation evidence contained about 47.8% of cellulose, 23.7% of hemicellulose, 25.9% of lignin, and 1.8% ash [36]. Thus, low ash and high lignin contents were observed, which are essential characteristics in producing activated carbon with optimal properties [37]. High lignin contents provided high yields, thereby contributing to the fixed carbon content at the end of the carbonization and activation processes [37]. Then, when analyzing the ultimate analysis results, it was observed that the carbon content from activated carbons had been risen from 50.86% to 75.81 wt%, as can be seen in Table 1. In activated carbon, hydrogen, nitrogen, sulfur, and oxygen contents decreased due to the decomposition during the pyrolysis and activation process. There were no significant differences between the palm fibres (stem and sheath) in carbon, hydrogen, and oxygen content. From the analyses, it was exhibited that the low ash content of the precursor makes it a good starting material for the preparation of activated carbon. The activated carbon yield ranged from

Table 1 Composition and properties of the materials

Samples	Proximate Analysis (wt.%)		Elemental Analysis (wt.%)					Density (g.cm^{-3})	Superficial area (m^2.g^{-1})
	Moisture (%)	Ash (%)	C	H	N	S	O		
*FIS	12.21	1.92	50.86	8.55	1.31	0.23	45.07	1.93	797
*FAS	10.73	1.81	48.01	8.43	1.25	0.19	42.13	2.20	791
*ACS	1.86	0.90	75.81	3.28	0.97	0.16	19.79	2.92	1102
*FIST	10.92	1.88	52.76	7.93	1.23	0.27	37.82	1.98	490
*FAST	9.85	1.69	53.69	7.89	1.12	0.23	37.08	2.14	349
*ACST	1.74	0.84	77.04	3.19	0.83	0.21	18.74	3.40	1172

*FIS (in natura fibre from sheath); FAS (activated fibre from sheath); ACS (activated carbon from sheath); FIST (in natura fibre from stem); FAST(activated fibre from stem); ACST (activated carbon from stem)

68.30 to 64.50% for ACS (activated carbon from sheath) and ACST (activated carbon from stem), respectively.

Figure 2 shows the surface morphological of fibres (*in natura* and activated) and activated carbon in different magnifications. It was observed a difference in the surface morphology of the *in natura* fibres (stem and sheath) compared to activated fibres, due to the NaOH activation that resulted in a well developed and uniform surface, producing an orderly pore structure. However, after the pyrolysis, the surface morphological of activated carbon presented an expanded state of pore structure due to the evaporation of the NaOH during carbonization, leaving the space previously occupied by the activation agent available for the adsorption of MB. All samples showed irregular and porous surfaces at depths that possibly allow the transport, entry, and adsorption of MB. Heidarnejad et al. [10] obtained similar behavior with activated carbons from the date the press cake by low-frequency ultrasound.

Different pores were observed in the activated carbon samples. Due to activation and carbonization, volatiles was removed, producing a fixed carbon mass with the widening of pore networks present in activated carbon samples [38]. Thus, the activated carbon presents an adequate morphology for MB adsorption. In general, carbon surfaces have irregular pores and well-developed pores on the surface of the activated carbon.

Porosity was measured via Hg porosimetry, as shown in Table 1. Each material density tends to be lower for *in natura* fibres (sheath and stem), presents the same tendency to increase for fiber activation (i.e. ≈ 10% of increases). Activated carbon exhibited a higher density increase, 51% for the sheath, and 71% for the stem palm, compared to *in natura* fibres. This behavior is a result of densification, confirming SEM images results.

The determination of surface area is an essential characteristic because it will result in higher sorption capacity [39]. Thus, both activated carbons (sheath and stem) presented a significant increase in surface area compared to *in natura* fibres, an improvement of 38% and 71% for sheath (ACS)

and stem (ACST) was observed, respectively. Consequently, the expected result of MB sorption capacity should be better for ACST showed higher superficial area than ACS and, respectively, higher superficial contact with MB.

Porosity characteristics directly influence the superficial area. For a better understanding of porosity analysis, Fig. 3 shows the histogram of pore size distribution. Thus, the average pore diameter revealed the macroporous structure of prepared activated carbon according to the IUPAC classification, indicating that the materials have a relatively large surface area, which is one of the prerequisites as excellent adsorption material, as can be seen in Fig. 2b.

A higher difference between *in natura* fibres and activated carbon showed that the stem palm (Fig. 3b) presented a higher frequency of larger porosity (> 40 μm) for *in natura* fibres. After activation of the fibres processes, larger porosities are broken into smaller voids. Activation of the carbon process densities the material and creates a homogeneity distribution of pore size, between small and larger porosity.

The same behavior was found for sheath palm fibres and activated carbon, which *in natura* fibres presented higher frequency for larger porosity (i.e. > 40 μm), with less frequency when compared to *in natura* fibres from stem. The first treatment (activated fibre) broke larger porosity into small one (i.e. < 15 μm), and then, the activated carbon densities the material (as shown in SEM images – Fig. 2), and created more homogeny distribution of pore size. The larger pore diameter is essential for initial oil sorption; although, it exhibits low retention capacity [40]. On the other hand, the smaller pore diameter is also relevant concerning capillary effects that create a sorption force, facilitating retention [40–42]. Considering previous porosity distribution for all materials, the activation of carbon results in pore size with homogeneity in a frequency distribution, presenting appropriated sorption characteristics.

FTIR analysis was used to identify some characteristic functional groups of activated carbon and fibres (*in natura* and activated) [12]. The analyzed spectra demonstrated the activating agent's ability to alter the chemical surface of

Fig. 2 **a** SEM of the palm fibres (superior view): (a) FIS (*in natura* fibre from sheath); (b) FIST (*in natura* fibre from stem); (c) FAS (activated fibre from sheath); (d) FAST(activated fibre from stem); (e) ACS (activated carbon from sheath); (f) ACST (activated carbon from stem); **b** graphical representation of different sizes of pores (macropores, mesopores, and micropores) in a lateral view
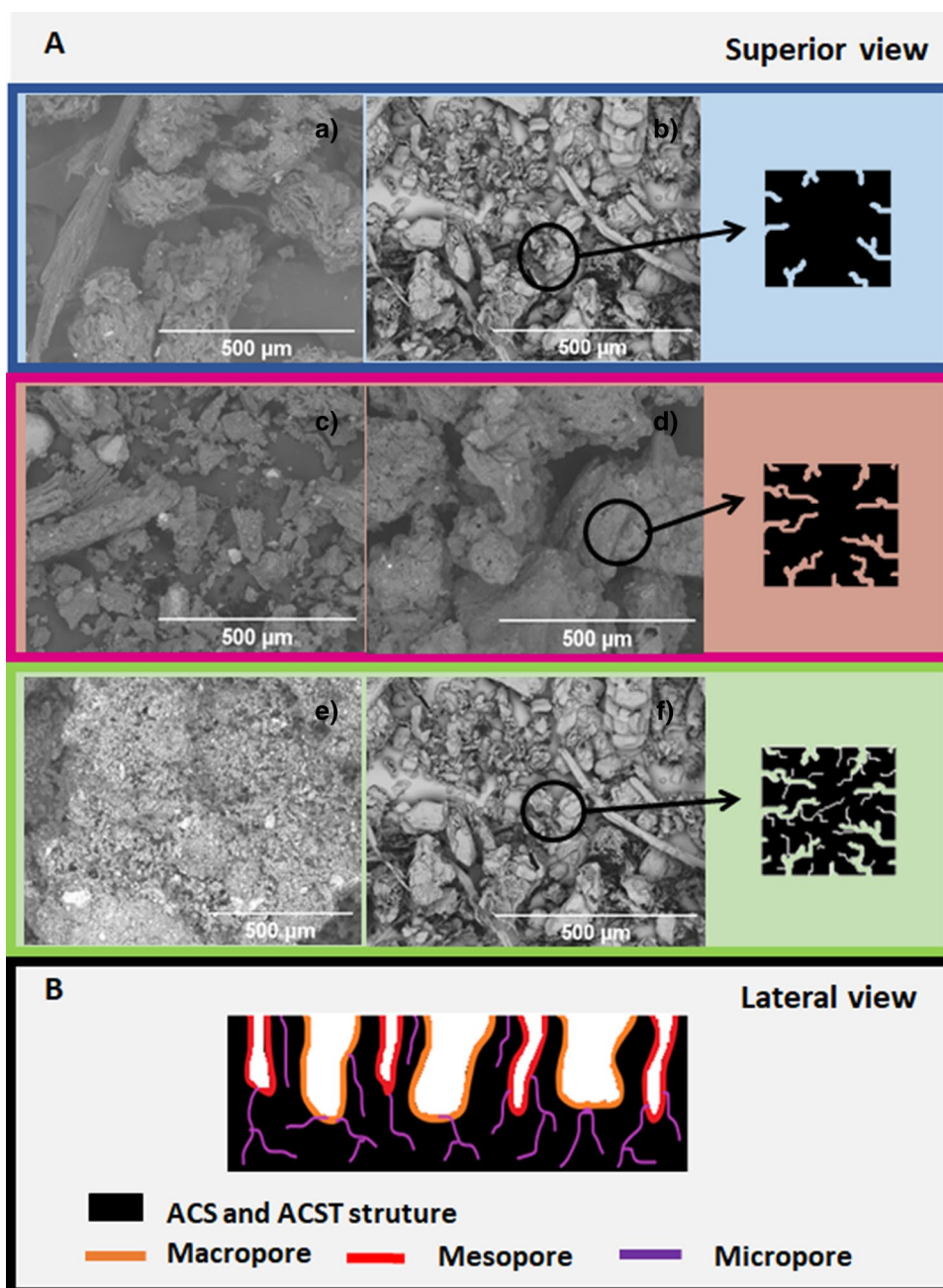
activated carbon, which could be detected from functional groups present in the sample (Fig. 4).

In *natura* fibres (stem and sheath), the FTIR spectra showed broadband situated about in the range $3500-3200$ cm^{-1} ascribed to O–H stretching vibration. The bands near 2920 and 1620 cm^{-1} corresponded to the stretching vibration of aliphatic C–H and aromatic C=C. Two bands at approximately 1160 and 1020 cm^{-1} related to stretching vibration of C–O bond in organic compounds (such as alcohols, phenols, acids, ethers or esters) [26]. Some bands associated with organic groups such as C–H and C–O bonds expressed the higher intensities for the spectrum

of activated fibres from stem. However, for the spectrum of activated fibres from sheath, these organic groups expressed the lower intensities.

After carbonization, all samples of activated carbon substantially decreased of band intensities such as in the range $3500-3200$ cm^{-1} vibration related to the O-H stretch bonded, alcohol, phenol functional group; 2920 and 1620 cm^{-1} related to stretching vibration of aliphatic C–H and aromatic C=C; and 1160 and 1020 cm^{-1} related to stretching vibration of C–O bond in organic compounds.

This behavior can be observed in several carbons obtained from natural fibres, which provides activated carbon with
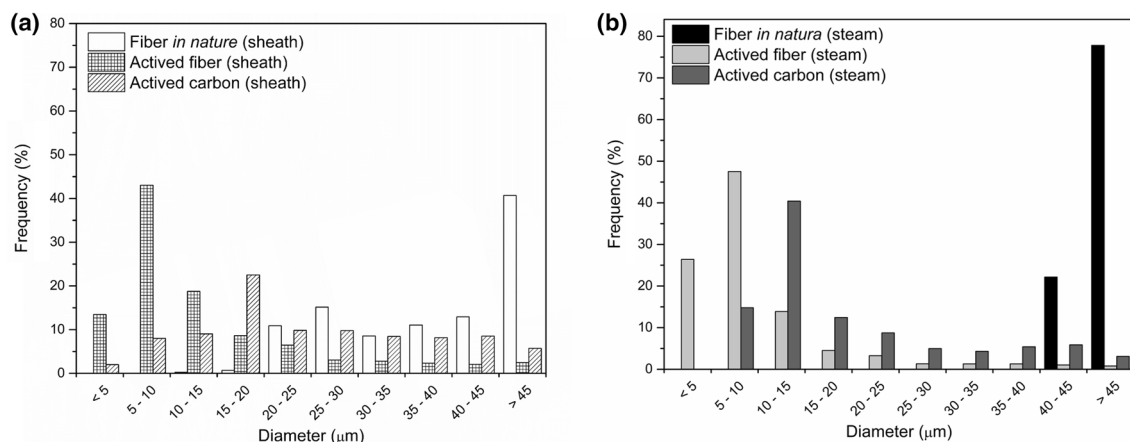
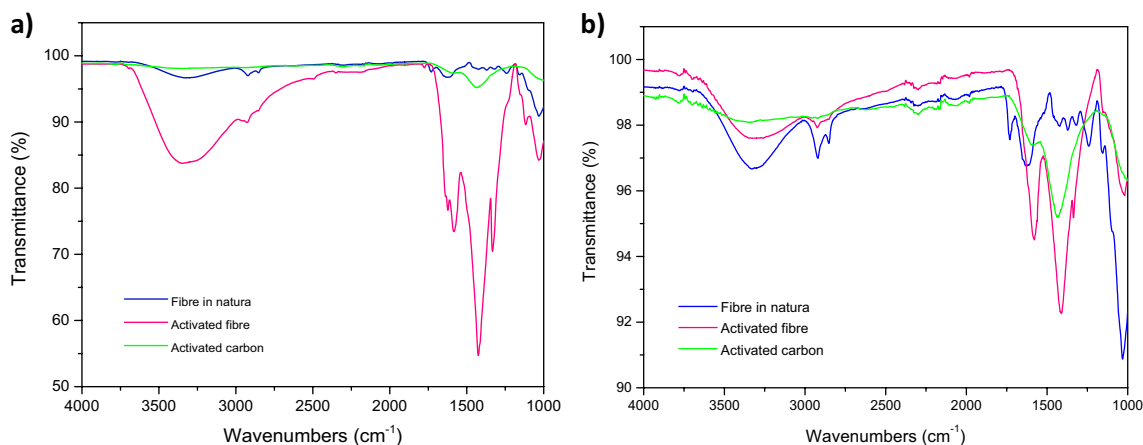**Fig. 3** Pore size distribution: **a** sheath and **b** stem

Fig. 4 FTIR of the palm fibres: **a** stem and **b** sheath

NaOH more significant natural substances, such as natural or synthetic pigments [38, 43]. This data corroborates the results obtained in the adsorption capacity of coal in methylene blue.

Similar vibration was observed in other works with activated carbon developed from green coconut shell, *ficus carica bast*, and date press cake by low-frequency ultrasound [10, 12, 38]. El-Shafey et al. [44] also observed a reduction of the band related to the -OH stretching vibration and, therefore, favored the methylene blue adsorption.

These changes in absorption bands suggest the interactions of stained cells with biosorbent functional groups [45].

Figure 5 evidences the TGA and DTG curves for the materials. The *in natura* and activated fibres presented two important weight loss steps. Between 30 and 120 °C, which is characteristic of the evaporation of water molecules adsorbed on the surface [1]. Mulinari et al. [46] obtained similar behavior with the sugarcane bagasse fibres. Another stage of weight loss was the thermal decomposition of the

cellulose structure, which was occurred at 260–350 °C. Somseta et al. [1] evidenced similar behavior when studying activated carbon/cellulose biocomposite films to remove MB.

Only a single weight loss step was observed in the activated carbon, which occurred near 100 °C.

Analyzing both curves showed that the activated carbon loses less weight loss than *in natura* and activated fibres in the same range temperature (Fig. 5). Thus, the activated carbon can be exposed to 600 °C without much significant weight loss adsorbent. However, it was noted that fibres from the sheath presented a minimal difference in thermal stability compared to fibres from the stem, which can be evidenced in Table 2.

Thus, it can be observed that, when comparing these results to the green coconut shell carbon, a greater thermal resistance was obtained because the weight loss of the sheath and stem was 17.69% and 20.96%, respectively, in the range 27 to 600 °C [38].
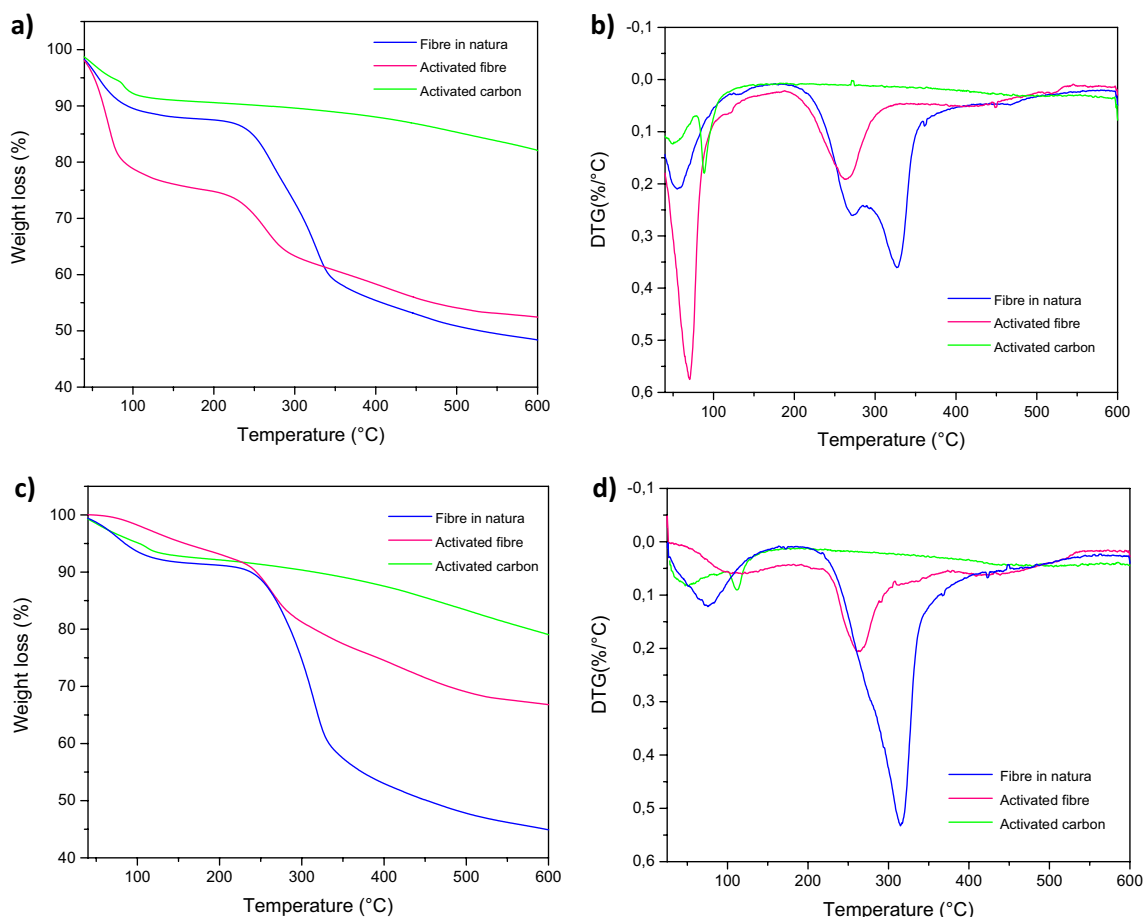
Fig. 5 TGA and DTG of the palm fibres: (**a** and **b**) sheath and (**c** and **d**) stem

Table 2 Weight loss at different temperatures and degradation temperature peak of materials

Samples	Weight loss (%)						Degradation temperature peak (°C)
	100 °C	200 °C	300 °C	400 °C	500 °C	600 °C	
FIS	10.46	12.51	27.33	44.61	49.16	51.64	307
FAS	21.16	25.22	36.70	41.69	45.91	47.57	251
ACS	7.83	9.42	10.40	11.99	14.7	17.96	---
FIST	6.46	8.83	25.51	47.04	52.21	55.11	312
FAST	1.82	6.92	18.77	25.47	30.98	33.21	268
ACST	4.89	7.88	9.67	12.49	16.70	20.96	---

FIS in natura fibre from sheath, *FAS* activated fibre from sheath, *ACS* activated carbon from sheath, *FIST* in natura fibre from stem, *FAST* activated fibre from stem, *ACST* activated carbon from stem

El-Shafey et al. [39] obtained a constant weight loss of about 22.1% between 120 and 785 °C, with maximum weight loss at 280 °C. Somsesta et al. [1] obtained thermal decomposition in the cellulose structure between 276 and 350 °C, showing that the activated carbon of the sheath and stem have greater resistance to high temperatures.

From diffractograms (Fig. 6) two peaks at angle 22° and 43° relayed to (002) and (100/101) lattice planes were noted for *in natura* and activated fibres (sheath and stem),

respectively. The broad peak at 22° is characteristic of disordered aromatic carbon structure, and the peak at 43.4° is characteristic of graphitic or organized carbon. The signal intensities of both materials' graphitic carbon are similar, indicating that their structures are also similar [15].

After the pyrolysis process, the disappearance of peaks was observed in both materials indicating the amorphous nature of the adsorbent, contributing to methylene blue removal [46]. Sahu et al. [22] evidenced similar results
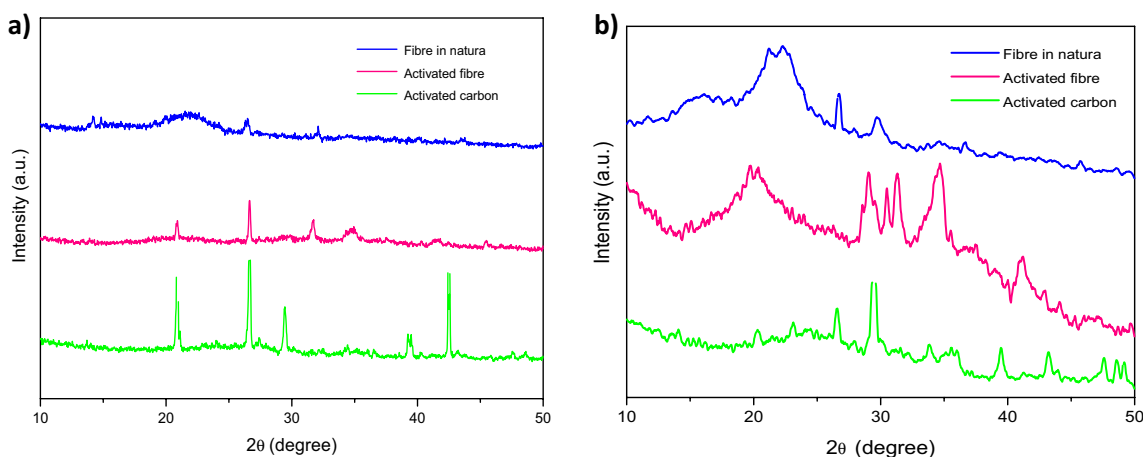
Fig. 6 XRD of the palm fibres: **a** sheath and **b** stem

Table 3 Removal of MB of the activated carbon from sheath and stem

Concentration	ACS (%)	ACST (%)
25	89.9	95.0
50	82.6	89.7
100	73.8	80.8
250	54.7	44.0
500	54.2	43.2

ACS activated carbon from sheath, *ACST* activated carbon from stem

when synthesizing activated carbon from kendu fruit peel by the carbonization and chemical activation with ammonium carbonate.

Effect of Concentration in the Removal Efficiency of Methylene Blue

The effect of concentration in removing MB (25 to 500 mg. L^{-1}) on activated carbon (stem and sheath) with a contact time of 1 h was varied. Table 3 shows that MB removal decreased with a higher concentration of adsorbent due to the increase in the driving force for mass transfer [12]. At low concentrations, there will be unoccupied active sites on the adsorbent surface. On the other hand, above optimal MB concentration, the active sites required for the dye's adsorption will lack, which can retard the MB adsorption by activated carbon. Pathania et al. [12] also observed similar behavior to study activated carbon developed from *Ficus carica bast* (FCBA).

The highest efficiency in the sorption carried out with the stem and sheath's activated carbon is 95% and 89.88% at 25 mg.L^{-1}. Ibupoto et al. [48] studied the reusable carbon nanofibres for MB removal for the removal efficiency

at 25 mg.L^{-1} and observed that in 15 min a removal of 85% occurred; and in 1 h a complete removal occurred, considering the equilibrium time to optimize parameters. Thus, compared to the activated carbon proposed in this work, it was demonstrated that the activated carbon from the stem and sheath obtained better adsorption performance than carbon nanofibres.

The adsorption capacity was evaluated using the Langmuir isotherm model. It has been observed that the sorption capacity (q_m) was found to be 110.79 and 162.54 mg.g^{-1} for stem and sheath palm, respectively (Table 4). However, to compare the separation factors RL, obtained from the isotherms, it was noticed that the MB sorption was more favorable for the activated carbon of the palm stem at lower concentrations (Fig. 7). This can be identified through the range of RL values, which were slightly lower than the carbon from the sheath, indicating a greater affinity between adsorbent and adsorbate (Table 4). When comparing the RL values with Doke et al. [49], both favor the adsorption process.

Table 5 shows the maximum adsorption capacity of MB on adsorbent obtained by Langmuir isotherm. It is possible to deduce that activated carbon from palm residue is a good precursor for producing efficient organic adsorbents with adequate adsorption capacity for MB dyes.

The pH value is one of the factors that influence the adsorption performance [1]. To understand the adsorption process was necessary to determine the pH_{ZPC} (the pH at which the net surface charge of the adsorbent is zero) of the adsorbent material [50]. Cationic dyes such as methylene blue and methyl violet are usually adsorbed minimally at low pH and exhibit increased adsorption with increasing pH [51]. This behavior is due to the electrostatic interaction between cationic dye molecules and anionic functional groups on the adsorbent's surface. Thus, the pH_{ZPC} of activated carbon
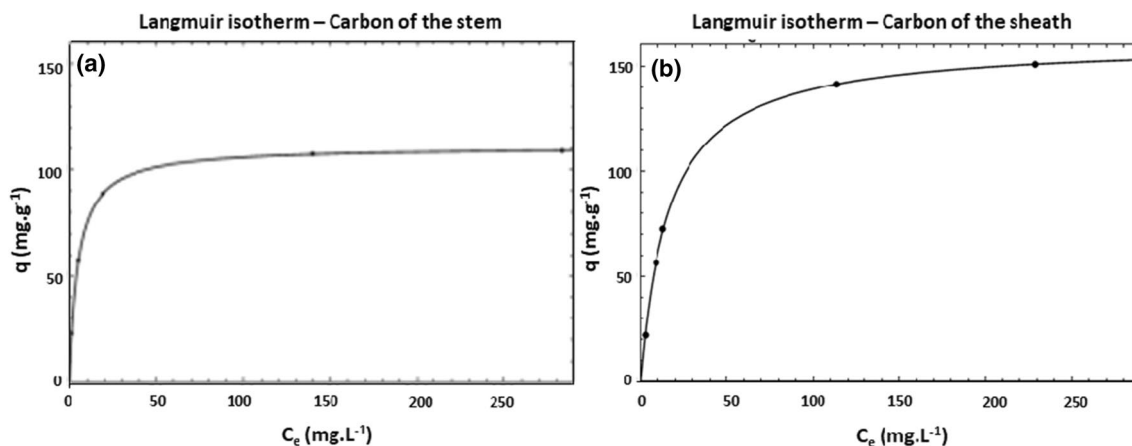
Fig. 7 Adsorption isotherms: **a** activated carbon from stem and **b** activated carbon from sheath

Table 4 Langmuir Isotherm coefficients

Fibres	Q_m (mg.g^{-1})	K_L (L.mg^{-1})	RL
Stem	110.79	0.21	0.016–0.792
Sheath	162.54	0.062	0.066–0.865

q_m (dye concentration when monolayer forms on biosorbent); K_L (Langmuir constant); RL (separation factor)

Table 5 Adsorption capacity of MB in mg per gram of the activated carbon from sheath and stem

Concentration	ACS (mg.g^{-1})	ACST (mg.g^{-1})
25	22.47	23.75
50	41.32	44.85
100	86.89	80.84
250	136.65	110.08
500	271.01	216.15

ACS activated carbon from sheath, *ACST* activated carbon from stem

(sheath and stem) was approximately 6, which means that the surface of the carbon is positively charged when the pH of the solution is lower than 6 and is negatively charged at pH values higher than 6, as can be seen in Fig. 8.

Therefore, as MB is a cationic dye, its adsorption will be favored by the more highly negatively charged activated carbon under alkaline conditions. When the pH of the dye solution increases, the positive charge at the interface of that solution decreases, and the negative charge appears on the adsorbent surface resulting in an increase in MB adsorption due to the more significant electrostatic attraction between the positively charged adsorbate and the negatively charged adsorbent [52]. The adsorption capacity increases in basic media due to the adsorption mechanism, which involves the interactions between cationic dye and negatively charged adsorbent surface. Oppositely, in acidic medium, the positively charged surface of sorbent tends to oppose the adsorption of the cationic adsorbate [12, 53–55]. The literature shows the performance in MB removal with pH ~ 7.0 and basic. In this work, the pH of the solution was adjusted to 6.
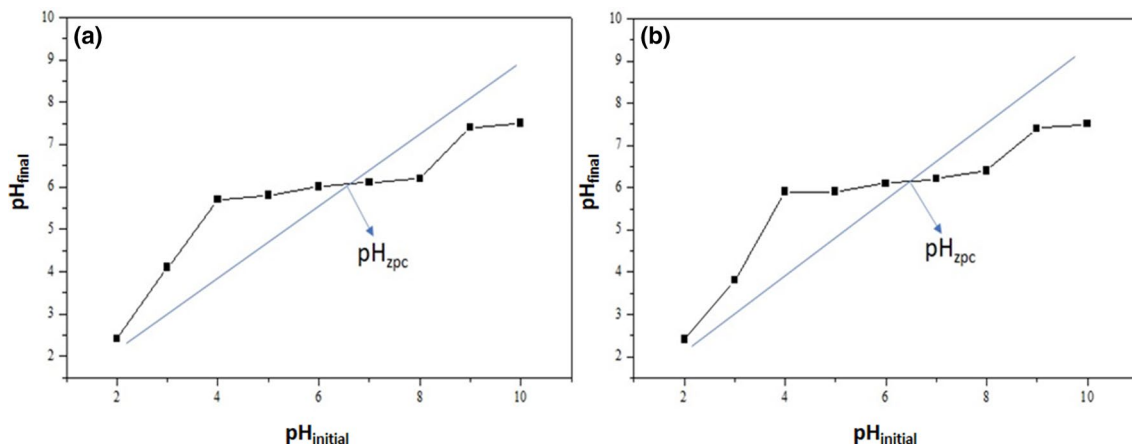

Fig. 8 pH$_{zpc}$ of the activated carbon: **a** sheath and **b** stem

Then, if the pH of the MB solution in this study is changed, it will be possible to increase the proposed adsorbent's removal efficiency.

Similar results have been reported in the literature by researchers with pH value ~ 6 or superior to 6 for MB removal [1, 12]. Li et al. [56] proposed methylene blue and aniline's adsorption onto activated carbon from waste edible fungus residue. These authors presented an adsorption capacity of MB superior to 95% with pH 6–10 at 100 mg.L^{-1} and an adsorbent dose of 40 mg. Saheed et al. [57] realized the sorption study of methylene blue on activated carbon prepared from jatropha curcas (JAC) and terminalia catappa seed coats (TAC). They observed that TAC presented a dye removal capacity of 25 mg.g^{-1} with pH 6 at 40 mg.L^{-1} and an adsorbent dose of 20 mg.

Effect of Contact Time in the Removal Efficiency of Methylene Blue

The effect of contact time in the removal of MB can be seen in Fig. 9. Analyzing the efficiency of activated carbon from the stem, the highest percentage rate of MB removal was 53.21% in 40 min (Fig. 9a). On the other hand, the efficiency

of activated carbon from sheath was 65.26% in 10 min for removing MB (Fig. 9b). It can also be seen that the dye adsorption capacity of the activated carbon of the stem is 26.61 mg.g^{-1} (Fig. 9c) and that of the activated carbon of the sheath is 32.63 mg.g^{-1} (Fig. 9d).

The adsorption rate change is because, initially, all the adsorbent sites are empty, and the solute concentration gradient is very high. Subsequently, the lower adsorption rate is due to a decrease in the number of vacant sites of adsorbent and dye concentrations. The decrease in adsorption particularly indicates a possible monolayer of MB in the adsorbent surface [45, 55]. This can be attributed to the lack of available active sites necessary for greater uptake after reaching equilibrium [45].

Figure 9 shows that in shorter contact times, MB's removal by the activated carbons is faster.

Somsesta et al. [1] analyzed MB's removal efficiency at 40 mg.L^{-1} and obtained a removal rate of 70%, considering pH 6.9, at 35 °C, and in 360 min.. Compared to the activated carbon proposed in this work, the sheath's activated carbon shows the removal of 65.26%, at 50 mg.L^{-1}, considering pH 6.0, at 25 °C in 10 min. In this way, the activated carbon of the sheath palm presents better adsorption results.
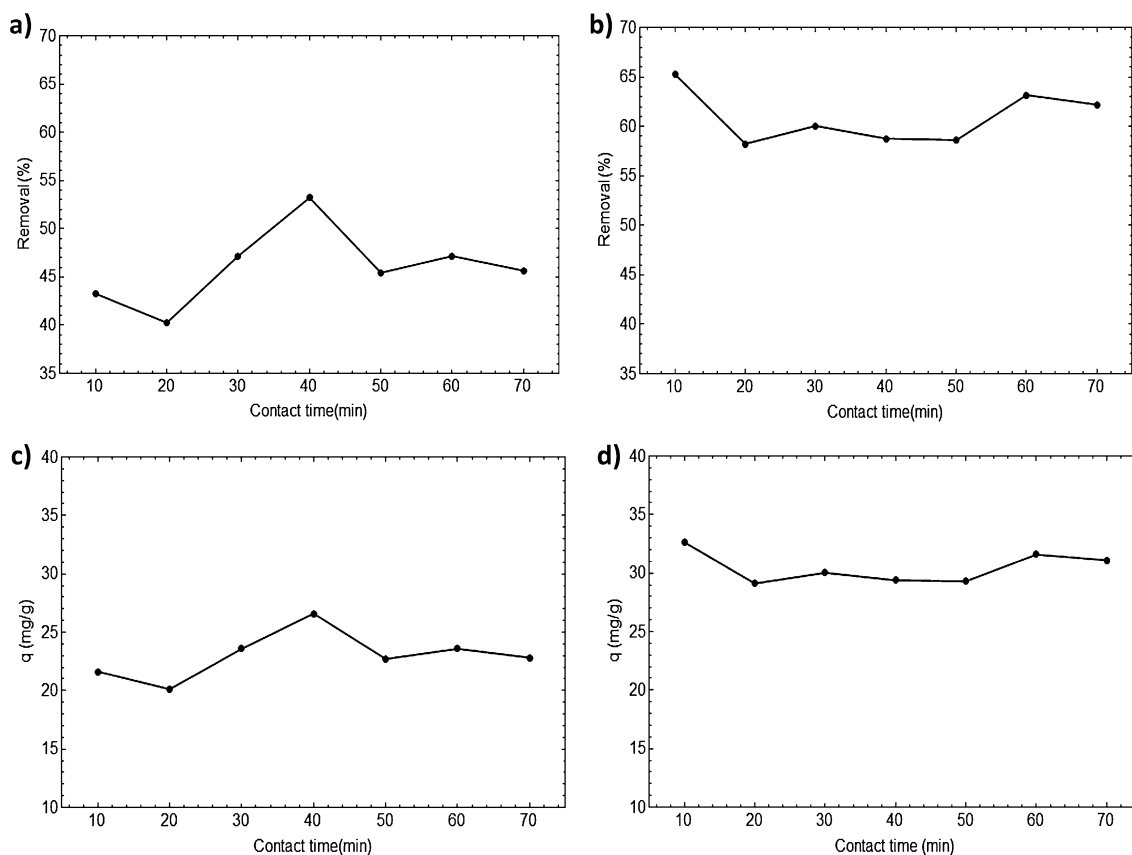

Fig. 9 Effect of contact time in the removal efficiency of methylene blue: **a** activated carbon from stem and **b** activated carbon from sheath; Effect of contact time on adsorption capacity: **c** activated carbon from stem and **d** activated carbon from sheath

Meili et al. [24] observed that the activated carbons from sugarcane bagasse and soursop could remove MB about 75% and 50% in 50 mg.L^{-1} solution for 60 min. Compared to the activated carbon proposed in this work, the stem and sheath obtained, respectively, 89.7% and 82.63% in 50 mg.L^{-1} solution. Then, the activated carbon of the stem and sheath palm present better adsorption results.

The adsorbent materials, once saturated, are directly discarded. However, several studies have shown the possibility of reusing these sorbents to minimize operating costs and product waste [12, 13]. Typically, regeneration techniques are selected according to the contaminant's nature, the operating cost, and the conditions of the processes [58]. All the studies exposed demonstrate favorable results for the process of regeneration and reuse of the adsorbent materials. It is possible to observe that, after a few adsorption-desorption cycles, the adsorption capacity of the activated carbon is reduced due to the occurrence of strong interactions between the dye molecules and the adsorbent [59].

Conclusion

Palm fibres from stem and sheath based activated carbon were successfully prepared by the chemical activation method with NaOH. The operating parameters for the maximum sorption were dye solution concentration (25 mg.L^{-1}), sorbent dosage (30 mg), contact time (60 min), and temperature (303 K). Both achieved removal efficiency greater than 85% at 25 mg.L^{-1}. The adsorption isotherm was well defined by the Langmuir model with a maximum adsorption capacity of 110.79 and 162.54 mg.g^{-1} for stem and sheath palm. The equilibrium data were well adjusted in the Langmuir isotherm model, which confirms that the adsorption is heterogeneous and occurred through physicochemical interactions. Of this form, the activated carbon from the sheath and stem of the palm has the characteristics necessary to use adsorbents to remove blue methylene.

Compliance with Ethical Standards

Conflict of interest The authors declare that they have no conflict of interest.

References

1. Somsesta N, Sricharoenchaikul V, Aht-Ong D (2020) Adsorption removal of methylene blue onto activated carbon/cellulose biocomposite films: Equilibrium and kinetic studies. Mater Chem Phys 240:122221. https://doi.org/10.1016/j.matchemphys.2019.122221

2. Wang G, Chen Y, Xu G et al (2019) Effective removing of methylene blue from aqueous solution by tannins immobilized on cellulose microfibers. Int J Biol Macromol 129:198–206. https://doi.org/10.1016/j.ijbiomac.2019.02.039

3. Conselho Nacional do Meio Ambiente. Resolução n.º 430, de 13 de maio de 2011. http://www.mma.gov.br/port/conama/legiabre., 2011 (accessed: 28 October 2019)

4. Conselho Nacional do Meio Ambiente, Resolução n.º 357, de 17 de março de 2005. http://www.mma.gov.br/port//conama/res/res05/res35705.pdf, 2005 (accessed 28 october 2019)

5. Youcef LD, Belaroui LS, López-Galindo A (2019) Adsorption of a cationic methylene blue dye on an Algerian palygorskite. Appl Clay Sci 179:105145. https://doi.org/10.1016/j.clay.2019.105145

6. Alfredo APC, Gonçalves GC, Lobo VS, Montanherb SF (2015) Adsorção de azul de metileno em casca de batata utilizando sistemas em batelada e coluna de leito fixo. RVQ 7:1909–1920. https://doi.org/10.5935/1984-6835.20150112

7. Liu S, Chen X, Ai W, Wei C (2019) A new method to prepare mesoporous silica from coal gasification fine slag and its application in methylene blue adsorption. J Clean Prod 212:1062–1071. https://doi.org/10.1016/j.jclepro.2018.12.060

8. Rezakazemia M, Shirazian S (2019) Lignin-chitosan blend for methylene blue removal: Adsorption modeling. J Mol Liq 274:778–791. https://doi.org/10.1016/j.molliq.2018.11.043

9. El Hajam M, Kandri NI, Harrach A et al (2019) Adsorption of Methylene Blue on industrial softwood waste "Cedar" and hardwood waste "Mahogany" comparative study. Mater Today Proceedings 13:812–821. https://doi.org/10.1016/j.matpr.2019.04.044

10. Heidarnejad Z, Rahmanian O, Fazlzadeh M, Heidari M (2018) Enhancement of methylene blue adsorption onto activated carbon prepared from Date Press Cake by low frequency ultrasound. J Mol Liq 264:591–599. https://doi.org/10.1016/j.molliq.2018.05.100

11. Li Z, Jia Z, Ni T, Li S (2017) Adsorption of methylene blue on natural cotton based flexible carbon fiber aerogels activated by novel air-limited carbonization method. J Mol Liq 242:747–756. https://doi.org/10.1016/j.molliq.2017.07.062

12. Pathania D, Sharma S, Singh P (2017) Removal of methylene blue by adsorption onto activated carbon developed from Ficus carica bast. Arab J Chem 10:1445–1451. https://doi.org/10.1016/j.arabjc.2013.04.021

13. Foo KY (2018) Effect of microwave regeneration on the textural network, surface chemistry and adsorptive property of the agricultural waste based activated carbons. Proc. Saf. Environ. Protec. 116:461–467. https://doi.org/10.1016/j.psep.2018.01.022

14. Chiang C-H, Chen J, Lin J-H (2020) Preparation of pore-size tunable activated carbon derived from waste coffee grounds for high adsorption capacities of organic dyes. J Environ Chem Eng 8:103929. https://doi.org/10.1016/j.jece.2020.103929

15. Beltrame KK, Cazetta AL, Souza PSC et al (2018) Adsorption of caffeine on mesoporous activated carbon fifibers prepared from pineapple plant leaves. Ecotoxicol Environ Saf 147:64–71. https://doi.org/10.1016/j.ecoenv.2017.08.034

16. Sarabandi D, Roudini G, Barahuie F (2019) Activated carbon derived from pine cone as a framework for the preparation of n-heptadecane nanocomposite for thermal energy storage. J Energy Storage 24:100795. https://doi.org/10.1016/j.est.2019.100795

17. El-Shafey EI, Ali SNF, Al-Busafii S, AL-Lawatih AJ (2016) Preparation and characterization of surface functionalized activated carbons from date palm leafflets and application for methylene blue removal. J Environ Chem Eng 4:2713–2724. https://doi.org/10.1016/j.jece.2016.05.015

18. Menya E, Olupot WP, Storz H (2018) Production and performance of activated carbon from rice husks for removal of natural organic matter from water A review. Chem Eng Res Des 129:271–296. https://doi.org/10.1016/j.cherd.2017.11.008

19. Enniya I, Rghioui L, Jourania A (2018) Adsorption of hexavalent chromium in aqueous solution on activated carbon prepared from apple peels. Sustain Chem Pharm 7:9–16. https://doi.org/10.1016/j.scp.2017.11.003

20. Sebron M, Gomez S et al (2020) Activated carbon from spent cofffee grounds as an adsorbent for treatment of water contaminated by aniline yellow dye. Ind Crops Prod 145:111953. https://doi.org/10.1016/j.indcrop.2019.111953

21. Sahu S, Pahi S, Sahu JK et al (2020) Kendu (Diospyros melanoxylon Roxb) fruit peel activated carbon—an efficient bioadsorbent for methylene blue dye: equilibrium, kinetic, and thermodynamic study. Environ Sci Pollut Res 27:22579–22592. https://doi.org/10.1007/s11356-020-08561-2

22. Yazdani MR, Duimovich N, Tiraferri A et al (2019) Tailored mesoporous biochar sorbents from pinecone biomass for the adsorption of natural organic matter from lake water. J Mol Liq 291:111248. https://doi.org/10.1016/j.molliq.2019.111248

23. Meili L, Lins PVS, Costa MT et al (2019) Adsorption of methylene blue on agroindustrial wastes: Experimental investigation and phenomenological modelling. Prog Biophys Mol Biol 141:60–71. https://doi.org/10.1016/j.pbiomolbio.2018.07.011

24. Han Q, Wang J, Goodman BA et al (2020) High adsorption of methylene blue by activated carbon prepared from phosphoric acid treated eucalyptus residue. Powder Technol 366:239–248. https://doi.org/10.1016/j.powtec.2020.02.013

25. Mulinari DR, Araujo MJF, Lopes GS (2015) Mechanical Properties of the Palm Fibers Reinforced HDPE Composites. World Acad Sci Eng Technol 2:824. https://doi.org/10.5281/zenodo.1109177

26. Mulinari DR, Guedes JR, Simba BG (2017) Low density polyethylene composites reinforced with Australian King Palm fibers: mechanical and thermal properties. Polym Bull 1:1–11. https://doi.org/10.1007/s00289-017-1963-9

27. Araujo MJF, Araujo MVF, Mulinari DR (2016) Evaluation of Biodegradability of a Compost Obtained from Polymeric Composite Reinforced Natural Fibers. Mater Sci Forum 869:265–269. https://doi.org/10.4028/www.scientific.net/MSF.869.265

28. Instituto Brasileiro de Geografia e Estatítca (2019) Produção Agrícola Municipal 2018. https://cidades.ibge.gov.br/brasil/pesquisa/15/0, (accessed: 14 June 2020).

29. Liu J, Yang X, Liu H et al (2020) Modification of calcium-rich biochar by loading Si/Mn binary oxide after NaOH activation and its adsorption mechanisms for removal of Cu(II) from aqueous solution. Colloids Surf A Physicochem Eng Asp 601:124960. https://doi.org/10.1016/j.colsurfa.2020.124960

30. Parre A, Karthikeyan B, Balaji A, Udhayasankar R (2020) Investigation of chemical, thermal and morphological properties of untreated and NaOH treated banana fiber. Mate Today Proceedings 22:347–352. https://doi.org/10.1016/j.matpr.2019.06.655

31. Takeuchi K, Fujishige M, Ishida N et al (2018) High porous bio-nanocarbons prepared by carbonization and NaOH activation of polysaccharides for electrode material of EDLC. J Phys Chem Solids 118:137–143. https://doi.org/10.1016/j.jpcs.2018.02.050

32. Chiang C-H, Chenb J, Lin J-H (2020) Preparation of pore-size tunable activated carbon derived from waste coffee grounds for high adsorption capacities of organic dyes. J Environ Chem Eng 8:103929. https://doi.org/10.1016/j.jece.2020.103929

33. Fallon PE, Rodriguez J, Wang JB (2017) QSWalk: A Mathematica package for quantum stochastic walks on arbitrary graphs. Comput Phys Commun 217:162–170. https://doi.org/10.17632/8rwd3j9zhk.1

34. Wolfram M (2020) https://www.wolfram.com/mathematica/, 2020 (accessed: 24 July 2020)

35. Erdogan SY, Önal Y, Akmil-Başar C et al (2005) Optimization of nickel adsorption from aqueous solution by using activated carbon prepared from waste apricot by chemical activation. Appl Surf Sci 252:1324–1331. https://doi.org/10.1016/j.apsusc.2005.02.089

36. Sousa TA, Habibe AF, Mulinari DR (2012) Caracterização das fibras da palmeira e do resíduo de fundição para produção de briquetes. Edição Especial do Curso de Mestrado Profissional em Materiais - junho/2012

37. Castro JP, Nobre JRC, Napoli A et al (2020) Pretreatment Affects Activated Carbon from Piassava. Polymers 12:1483. https://doi.org/10.3390/polym12071483

38. Das D, Samal DP, Meikap BC (2015) Preparation of Activated Carbon from Green Coconut Shell and its Characterization. J Chem Eng Process Technol 6:248. https://doi.org/10.4172/2157-7048.1000248

39. Rovira M, Giménez J, Martínez M et al (2008) Sorption of selenium (IV) and selenium (VI) onto natural iron oxides: goethite and hematite. J Hazard Mater 150:279–284. https://doi.org/10.1016/j.jhazmat.2007.04.098

40. Wei QF, Mather RR, Fotheringham AF, Yang RD (2003) Evaluation of nonwoven polypropylene oil sorbents in marine oil-spill recovery. Mar Pollut Bull 46:780–783. https://doi.org/10.1016/S0025-326X(03)00042-0

41. Alvarez JO, Saputra IWR, Schechter DS (2018) The Impact of Surfactant Imbibition and Adsorption for Improving Oil Recovery in the Wolfcamp and Eagle Ford Reservoirs. SPE J 23:2103–2117. https://doi.org/10.2118/187176-PA

42. Shen Y, Ge H, Meng M et al (2017) Effect of Water Imbibition on Shale Permeability and Its Influence on Gas Production. Energ Fuel 31:4973–4498. https://doi.org/10.1021/acs.energyfuels.7b00338

43. Hirata M, Kawasaki N, Nakamura T et al (2002) Adsorption of dyes onto carbonaceous materials produced from coffee grounds by microwave treatment. J Colloid Interface Sci 254:17–22. https://doi.org/10.1006/jcis.2002.8570

44. El-Shafey EI, Ali SNF, Al-Busafifi S, AL-Lawatih AJ (2016) Preparation and characterization of surface functionalized activated carbons from date palm leaflflets and application for methylene blue removal. J Environ Chem Eng 4:2713–2724. https://doi.org/10.1016/j.jece.2016.05.015

45. Liang S, Guo X, Feng N, Tian Q (2010) Isotherms, kinetics and thermodynamic studies of adsorption of Cu2 + from aqueous solutions by Mg2+/K + type orange peel adsorbent. J Hazard Mater 174:756–762. https://doi.org/10.1016/j.jhazmat.2009.09.116

46. Mulinari DR, Voorwald HJC, Cioffi MOH, Silva MLCP (2016) Cellulose fiber-reinforced high-density polyethylene composites–Mechanical and thermal properties. J Compos Mater 1:1–9. https://doi.org/10.1177/0021998316665241

47. Krishnamoorthy R, Govindan B, Banat F et al (2019) Date pits activated carbon for divalent lead ions removal. J Biosci Bioeng 128:88–97. https://doi.org/10.1016/j.jbiosc.2018.12.011

48. Ibupoto AS, Qureshi UA, Ahmed F et al (2018) Reusable carbon nanofifibers for efficient removal of methylene blue from aqueous solution. Chem Eng Res Des 136:744–752. https://doi.org/10.1016/j.cherd.2018.06.035

49. Doke KM, Khan EM (2017) Equilibrium, kinetic and diffusion mechanism of Cr(VI) adsorption onto activated carbon derived from wood apple shell. Arab J Chem 10:252–260. https://doi.org/10.1016/j.arabjc.2012.07.031

50. Mullick A, Neogi S (2016) Synthesis of potential biosorbent from used stevia leaves and its application for malachite green removal from aqueous solution: kinetics, isotherm and regeneration studies. RSC Adv 6:65960–65975. doi:https://doi.org/10.1039/C6RA15225B

51. Kaewsarn P, Saikaew W, Wongcharee S (2008) Dried Biosorbent Derived from Banana Peel: A Potential Biosorbent for Removal of Cadmium Ions from Aqueous Solution. The 18th Thailand Chemical Engineering and Applied Chemistry Conference October 20–21, 2008. https://www.researchgate.net/publication/317614977

52. Kumar A, Jena HM (2016) Removal of methylene blue and phenol onto prepared activated carbon from Fox nutshell by chemical activation in batch and fixed-bed column. J Clean Prod 137:1246–1259. https://doi.org/10.1016/j.jclepro.2016.07.177

53. Efimov MN, Vasilev AA, Muratov DG et al (2019) IR radiation assisted preparation of KOH-activated polymer-derived carbon for methylene blue adsorption. J Environ Chem Eng 7:103514. https://doi.org/10.1016/j.jece.2019.103514

54. El-Latif MMA, Ibrahim AM (2009) Adsorption, kinetic and equilibrium studies on removal of basic dye from aqueous solutions using hydrolyzed oak sawdust. Desalin Water Treat 6:252–268. https://doi.org/10.5004/dwt.2009.501

55. Nemr AE, Abdel WO, Amany ES, Khaled A (2009) Removal of direct blue-86 from aqueous solution by new activated carbon developed from orange peel. J Hazard Mater 161:102–110. https://doi.org/10.1016/j.jhazmat.2008.03.060

56. Li H, Liu L, Cui J et al (2020) High-efficiency adsorption and regeneration of methylene blue and aniline onto activated carbon from waste edible fungus residue and its possible mechanism. RSC Adv 10:14262. https://doi.org/10.1039/d0ra01245a

57. Saheed IO, Adekola FA, Olatunji GA (2017) Sorption Study of Methylene Blue on Activated Carbon Prepared from Jatropha curcas and Terminalia catappa Seed Coats. JOTCSA 4:375–394. https://doi.org/10.18596/jotcsa.287337

58. Gamal ME, Mous AH, El-Naas MH et al (2018) Bio-regeneration of activated carbon: A comprehensive review. Sep Purif Technol 197:345–359. https://doi.org/10.1016/j.seppur.2018.01.015

59. Carvalho DS, Cionek CA, Barros MASD, Arroyo PA (2015) Estudo da adsorção e dessorção do corante azul reativo BF5G em carvão ativado de osso. Blucher Chemical Engineering Proceedings https://doi.org/10.5151/chemeng-cobeq2014-0337-25946-164750

Affiliations

Lana S. Maia[1] · Andressa I. C. da Silva[1] · Emanuel S. Carneiro[1] · Francisco Maciel Monticelli[2] · Fernanda R. Pinhati[1] · Daniella R. Mulinari[3]

1. Departament of Chemistry and Environmental, Universidade do Estado do Rio de Janeiro, Resende, Brazil

2. Department of Materials and Technology, Guaratinguetá School of Engineering, São Paulo State University (Unesp), Guaratinguetá, Brazil

3. Department of Mechanicaland Energy, Universidade do Estado do Rio de Janeiro, Rodovia Presidente Dutra km 298, Polo Industrial, CEP 27537-000 Resende, Brazil